JOURNAL OF GEOPHYSICAL RESEARCH, VOL. 115, B01204, doi:10.1029/2009JB006466, 2010

Effect of strain localization on frictional behavior of sheared granular materials

Andrew P. Rathbun[1] and Chris Marone[1]

Received 17 March 2009; revised 30 July 2009; accepted 7 October 2009; published 26 January 2010.

[1] We performed laboratory experiments to investigate shear localization and the evolution of frictional behavior as a function of shear strain. Experiments were conducted on water-saturated layers, 0.3–1 cm thick, of Caesar till, a granular material analogous to fault gouge. We used the double-direct shear configuration at normal stresses ranging from 0.5 to 5 MPa and shearing velocities of 10–100 μm/s. Shear localization was assessed via strain markers and two proxies: (1) macroscopic layer dilation in response to perturbations in shear stress and (2) rate/state friction response to shear velocity perturbations. In creep mode experiments, at constant shear stress, we monitored dilation for perturbations in shear stress. In standard friction tests, we measured the coefficient of friction during perturbations in macroscopic strain rate. We find evidence of strain localization beginning at shear strain $\gamma \approx 0.15$ and continuing until $\gamma \approx 1$. Analysis of strain markers supports interpretations based on the proxies for localization and shows that strain is localized in zones of finite thickness. We also investigate symmetry of the friction response to step changes in imposed slip velocity and find that the behavior is symmetric. Our results favor the Ruina law for friction state evolution in which slip is the fundamental variable rather than the Dieterich law. The critical slip distance for friction evolution, D_c, is $\sim$140 μm. The Dieterich state evolution law requires different values of D_c for velocity increases/decreases, 100 μm versus 175 μm, respectively, and would imply strain localization/delocalization associated with shear in a finite zone.

Citation: Rathbun, A. P., and C. Marone (2010), Effect of strain localization on frictional behavior of sheared granular materials, *J. Geophys. Res.*, *115*, B01204, doi:10.1029/2009JB006466.

1. Introduction

[2] The localization of strain in brittle shear zones has broad implications for the seismic and aseismic nature of tectonic faulting and the rheology of subglacial till. Cataclasitic processes, wear, and reworking of sediments form fault gouge and its analog in the deforming substrate of some glaciers, subglacial till. Field observation of brittle shear zones [e.g., *Logan et al.*, 1979; *Arboleya and Engelder*, 1995; *Chester and Chester*, 1998; *Cashman and Cashman*, 2000; *Faulkner et al.*, 2003; *Hayman et al.*, 2004; *Fossen et al.*, 2007; *Cashman et al.*, 2007], laboratory experiments [e.g., *Mandl et al.*, 1977; *Logan et al.*, 1979, 1992; *Marone et al.*, 1990; *Gu and Wong*, 1994; *Beeler et al.*, 1996; *Scruggs and Tullis*, 1998; *Niemeijer and Spiers*, 2005], and numerical simulations [e.g., *Antonellini and Pollard*, 1995; *Morgan and Boettcher*, 1999; *Mair and Abe*, 2008] show that slip often localizes into discrete zones or along distinct fabrics in the shear zone.

[3] Field observations from exhumed brittle shear zones indicate that large slip (tens of kilometers) may occur in zones that range in width from a few centimeters to tens of meters [*Mooney and Ginzburg*, 1986; *Montgomery and Jones*, 1992; *Chester and Chester*, 1998; *Storti et al.*, 2003; *Sibson*, 2003; *Wibberley and Shimamoto*, 2003; *Billi and Storti*, 2004; *Chester et al.*, 2004; *Di Toro et al.*, 2005]. Fault zones grow in width by continued slip and evolve internally due to grain size reduction and mineral growth along shear bands [e.g., *Engelder*, 1974; *Scholz*, 1987; *Schleicher et al.*, 2006]. Such faults often include highly localized principal slip zones, which are hosted in fault damage regions and gouge zones. Fault zone width is difficult to quantify and exhibits extreme variation along strike, even for a single fault, but generally ranges from centimeters to hundreds of meters or more [e.g., *Scholz*, 2002; *Sibson*, 2003].

[4] Rate and state friction have been used to describe the behavior of brittle faulting in gouge and rocks [*Dieterich*, 1979, 1981; *Ruina*, 1983] based on the idea that stick-slip motion and interseismic creep are analogs for the seismic cycle [*Brace and Byerlee*, 1966]. Frictional instability requires that faults weaken with either increased slip (slip weakening) or increased velocity (velocity weakening). If the rate of weakening exceeds a critical value, elastic strain energy is released from the surrounding materials, causing

[1]Rock and Sediment Mechanics Laboratory, Penn State Center for Ice and Climate, Pennsylvania State University, University Park, Pennsylvania, USA.

0148-0227/10/2009JB006466$09.00

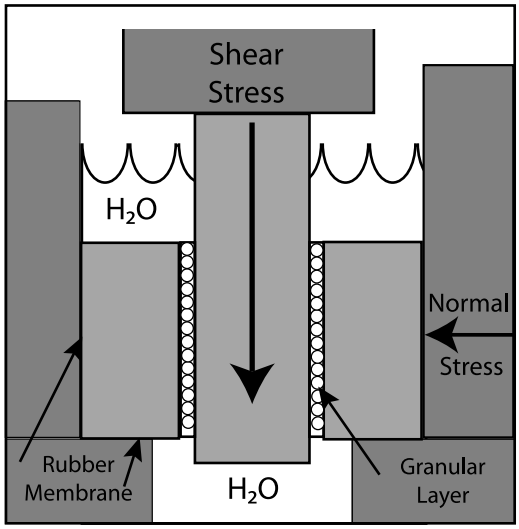

Figure 1. Double-direct shear configuration. The nominal frictional contact area was 10 cm × 10 cm and did not change with shear. Initial layer thickness was 0.3, 0.5, or 1 cm. The block arrangement was surrounded by a rubber membrane and filled with water. The reservoir was open to the atmosphere leading to saturated, drained conditions.

shear heating and elastic wave radiation. The critical weakening rate depends on the normal stress and elastic properties of the fault region [e.g., *Scholz*, 2002]. For deformation zones that exhibit increased frictional strength with increasing strain rate (so-called velocity strengthening frictional behavior), aseismic slip and creep are expected. Such behavior is expected for pervasive deformation prior to strain localization [*Marone et al.*, 1990, 1992]. The term creep is often used in two different contexts; in this study, we will use the word creep to denote deformation under constant shear stress, rather than to distinguish aseismic from seismic slip. In a granular material, pervasive shear and velocity strengthening frictional behavior have been attributed to the dilational work required to expand the layer [*Mead*, 1925; *Frank*, 1965; *Marone et al.*, 1990].

[5] Many of the processes that govern friction and strain localization in fault gouge also appear to be important in subglacial till. Shear deformation within till accounts for a large portion of the net displacement of some fast moving glaciers and ice streams [e.g., *Clarke*, 2005]. The rheology of subglacial till has been a matter of much debate; see *Alley* [2000] and *Clarke* [2005] for recent reviews. Early investigators used a power law relationship for glacial till where strain rate is proportional to shear stress raised to a stress exponent, n [e.g., *Boulton and Hindmarsh*, 1987]. For convenience, most modeling studies have assumed that till behaves as a viscous material with n of order 1, whereas most laboratory studies report a frictional (often termed "plastic") rheology of $n > 15$ [e.g., *Kamb*, 1991; *Iverson et al.*, 1997, 1998]. Work by *Rathbun et al.* [2008] shows that the rheology of till evolves from $n < 10$ to $n > 50$ from the onset of motion to steady frictional sliding. Recent studies show that glaciers exhibit stick-slip motion in some cases [*Anandakrishnan and Bentley*, 1993; *Ekstrom et al.*, 2003, 2006] and physical models have been proposed [*Tsai et al.*, 2008; *Winberry et al.*, 2009]. Basal tills are often characterized by zones of localized shear, [e.g., *Truffer et al.*, 2000; *Kamb*, 2001; *Evans et al.*, 2006; *Menzies et al.*, 2006] and laboratory studies indicate that till rheology is governed, in part, by the distribution of strain localization [*Larsen et al.*, 2006; *Thomason and Iverson*, 2006; *Iverson et al.*, 2008; *Rathbun et al.*, 2008]. However, there are relatively few detailed laboratory studies of strain localization and its effect on friction constitutive properties of till.

[6] Laboratory studies focused on earthquake faulting have shown that fault gouge often exhibits a transition from pervasive to localized deformation with increasing strain and that this transition coincides with a change from stable to stick-slip frictional sliding [e.g., *Logan et al.*, 1979, 1992; *Marone et al.*, 1990; *Beeler et al.*, 1996; *Marone*, 1998]. Similar connections between strain localization and frictional properties are emerging from studies of glacial till [e.g., *Iverson et al.*, 2008; *Rathbun et al.*, 2008]. However, most studies of till do not include direct information on friction constitutive behavior or stick-slip.

[7] The purpose of this paper is to report on laboratory investigations of strain localization and its influence on frictional behavior of till and granular fault gouge. We employ both constant shear velocity and constant shear stress boundary conditions, with careful attention to the influence of shear fabric development on frictional strength, layer dilation, and rate/state friction properties including the critical slip distance and steady state frictional strength.

2. Experimental Methods

[8] Experiments were performed in a servohydraulic, biaxial testing apparatus using the double-direct shear configuration (Figure 1). Two granular layers were sheared simultaneously between three steel forcing blocks at constant normal stresses of 0.5, 1, and 5 MPa (Table 1). The horizontal ram of the testing machine applies a constant normal force and the vertical ram imposes shear traction. Both rams can operate in stress or displacement servocontrol. Layer dimensions were 10 cm × 10 cm (nominal frictional contact area) × a thickness of 0.3, 0.5, or 1 cm (Table 1). Forcing blocks were grooved to a depth of 0.8 mm with wavelength of 1 mm perpendicular to shear to ensure that deformation occurred within the layer and not at the layer-block interface.

[9] Granular layers were constructed by applying a wall of cellophane tape around the forcing blocks to the desired layer thickness. The sample was then added and planed off to the desired thickness using a precision leveling jig (Table 1). This method produced constant initial layer thickness to a tolerance of ±0.2 mm. To reduce material loss along the front/back layer edges, guide plates were attached to the side forcing blocks. Molybdenum lubricant was used beneath the side forcing blocks to facilitate motion and layer dilation/compaction at constant normal stress. To further reduce material loss, a 0.01″ latex sheet was applied to the underside of the blocks. Calibration experiments show that the latex sheet adds <20 N (2 kPa) to the measured shear force [*Carpenter*, 2007] and we correct for this effect along with the gravitational force associated with the mass of the center forcing block (19 N).

Table 1. Experiment Details[a]

Experiment	σ_n (MPa)	Experiment Type	h_i (mm)	γ_i
p729	1	Creep- 2% steps	10	1.12
p731	1	Creep- 5% steps	10	1.15
p732	1	Creep- 5% steps	10	1.12
p737	1	Creep- 2% steps	10	1.13
p746	1	Creep- 2% steps	10	1.19
p750	1	Creep- 5% steps	10	1.14
p757	1	Creep- 5% steps	10	0.1
p760	1	Creep- 2% steps	10	0.18
p761	1	Creep- 5% steps	10	0.16
p1125	1	Creep- 5% steps	10	0.15
p1131	1	Creep- 5% steps	10	0.25
p1167	1	Creep- 5% steps	10	0; 2.65
p1194	1	Creep- 5% steps	10	0.19; 1.78
p1215	1	Creep- 5% steps	5	0.25
p1216	1	Creep- 5% steps	5	0.95
p1228	1	Creep- 5% steps	10	0.56
p1229	1	Creep- 5% steps	5	0.3
p1230	5	Creep- 5% steps	10	0.87
p1231	5	Creep- 5% steps	10	0.3
p1253	0.5	Creep- 5% steps	10	1.05
p1263	0.5	Creep- 5% steps	10	0.09
p1345	1	V-Steps- 10–30 μm/s	10	NA
p1494[b]	1	Constant Displacement	10	NA
p1507	1	V-Steps- 10–30 μm/s	10	NA
p1508[b]	1	V-Steps- 10–30 μm/s	10	NA
p1513	1	Creep- 5% steps	10	0.52
p1572	1	V-Steps- 10–30 μm/s	10	NA
p1814	1	Creep-7.5% steps	10	0.24; 1.27
p1824	1	Creep- 5% steps	10	1.07
p1906	1	Creep- 5% steps	10	1.17
p1910	1	Creep- 5% steps	3	0.7
p1938	1	Creep- 5% steps	10	0.17; 0.56
p1940	1	Creep- 5% steps	3	0.15; 0.92
p1942	1	Creep- 5% steps	10	4.3

[a]The parameter h_i is initial layer thickness and γ_i is initial shear strain. NA, not applicable.
[b]Experiments that included strain markers.

[10] Strain markers were constructed in select experiments (Table 1) by placing three sets of brass sheets (0.005″ thick) at equally spaced increments in the layer. Each set was filled with a 2 mm wide layer of blue sand (Kelly's Crafts, Inc.) and then the brass sheets were removed leaving a strip blue sand in the layer. The bulk weight percentage of markers was kept <5% to ensure that this material did not impact bulk frictional strength of the layer [e.g., *Logan and Rauenzahn*, 1987].

[11] All experiments were conducted under nominally saturated conditions by submerging the sample in water using a flexible rubber membrane (Figure 1). The reservoir was left open to the atmosphere at the top, resulting in saturated drained conditions for the layer. Before the application of stress, the sample was allowed to equilibrate with water for at least 45 min to ensure complete saturation.

[12] Normal and shear forces were measured with BeCu load cells to 0.1 kN resolution. Displacements were measured by direct current displacement transducers (DCDTs) to 0.1 μm resolution. Experiments were recorded with 24-bit analog-to-digital precision. We used a recording rate of 10 kHz and averaged samples for storage at >10 sample per micron of shear displacement in all experiments. Shearing velocity was computer-controlled via an analog servo command signal updated at 100 Hz. The initial layer thickness was measured, in situ under load, to ±0.01 mm. Measured displacements normal to the layer correspond to changes in layer thickness at constant normal stress. Both normal and shear displacements reported here have been corrected for the elastic stiffness of the vertical and horizontal load frames, 5 and 3.7 MN/cm, respectively. We measure macroscopic shear strain of the layer by integrating the measured slip increments, imposed at the layer boundaries, and dividing by the instantaneous layer thickness

$$\gamma = \sum_{j=1}^{X_{\max}} \frac{x_j - x_{j-1}}{h_j}, \tag{1}$$

where γ is bulk shear strain, x_j is the position of the center forcing block (e.g., shear offset at the layer edge), h is the instantaneous thickness at slip increment j, and $X_{\max}$ is the total displacement.

[13] The experiments were conducted using Caesar till, which is a mixed grain size granular material that derives from the Scioto (Ohio) Lobe of the Laurentide Ice Sheet and dates to about 19,500 years ago [*Haefner*, 1999]. Samples were air-dried and then disaggregated by hand before grain size analysis following the procedures of *Rathbun et al.* [2008]. We sieved the till and removed the >1 mm fraction in order to preserve stress homogeneity at our layer boundaries and to ensure that deformation was representative of the sample as a whole, rather than a few large grains. The experimental grain size was 98.7% sand, 1.2% silt, and 0.1% clay-sized grains (Figure 2) with some grains composed of aggregations of several small particles. Grain sizes less than 63 μm were analyzed using laser obscuration in a Malvern Mastersizer. Sample composition was determined via X-ray diffraction [*Underwood et al.*, 2003], with relative abundances of 35% quartz, 26% calcite, 23% plagioclase, and 16% clay minerals with the clay particles composed of 35.3% smectite, 38.5% illite, and 26.1% chlorite/kaolinite.

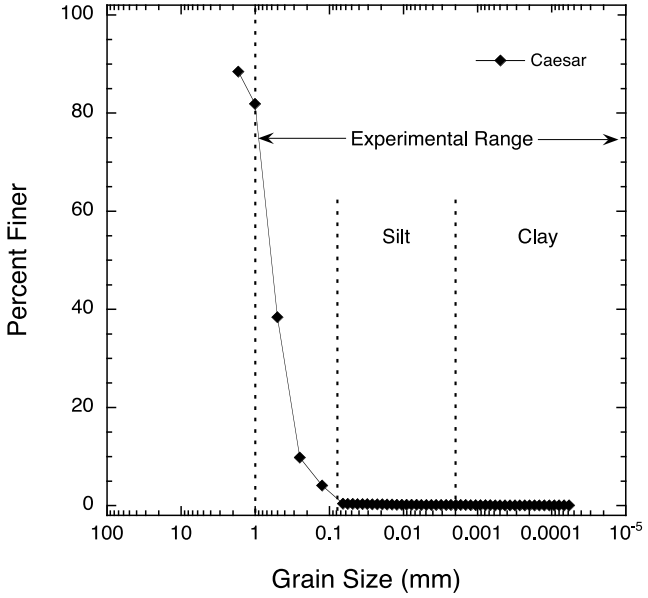

Figure 2. Grain size distribution for Caesar till. Samples were air-dried and sieved. Fine fraction (<63 μm) was analyzed using laser diffraction. Experiments are conducted on all grains that passed through a 1 mm sieve.

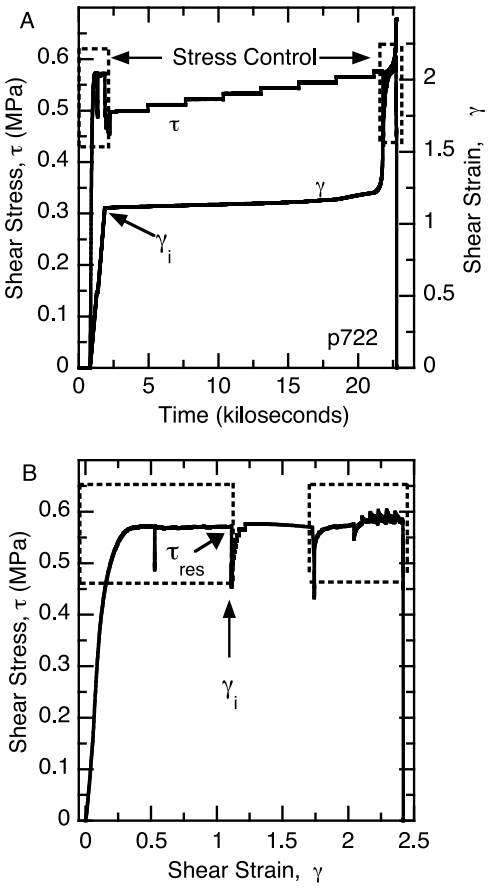

Figure 3. Complete stress-strain history for a representative experiment. Layers were sheared under controlled shear stress or constant shear displacement rate (boxed areas). (a) Shear stress and strain versus time to highlight creep mode section. (b) Shear stress versus shear strain for the same experiment. The preconditioning shear strain, γ_i was varied systematically to study the effect of shear localization on creep behavior. We measured τ_{res} during the (preconditioning) run-in, prior to creep tests under stress control. After completion of creep testing, we switched back to constant shear displacement rate. Modified from *Rathbun et al.* [2008].

2.1. Procedure for Monitoring Strain Localization

[14] Strain localization and shear fabric evolution were investigated by direct observation of preserved samples, postshear, and by indirect metrics measured in situ during the experiment. Layers were impregnated with epoxy for microstructural evaluation and tracking of strain markers. Experiments at low normal stresses and with granular particles typically do not show a well-developed shear fabric [e.g., *Mair and Marone*, 1999]. Therefore, we developed indirect methods of fabric characterization based on the layer response to perturbations in shearing rate and shear stress. These include layer dilation, friction memory effects characterized by the critical slip distance, and the steady state rate dependence of kinetic friction.

[15] Layer dilation was used as a proxy for strain localization. That is, we assume that only the fraction of the layer undergoing active strain exhibits shear dilation upon a perturbation in loading rate. Pervasive shear, in which the whole layer is actively involved in shear, results in larger dilation than localized shear, in which only a fraction of the layer is actively involved in shear. We measure dilation after accounting for geometric thinning of the layer in direct shear [*Scott et al.*, 1994].

3. Procedure, Results, and Analysis of Experiments

[16] We conducted two types of experiments for this study (Figure 3): (1) creep mode tests in which layers were sheared at a controlled shear stress value and (2) standard friction tests in which layers were sheared at a controlled shear displacement rate.

3.1. Creep Experiments

[17] Creep mode shearing (Figure 3a) began by first measuring steady state frictional strength, τ_{res} (Figure 3b) at constant shear displacement rate. We refer to the shear strain that accumulated prior to creep loading as preconditioning shear strain, γ_i, and we varied γ_i from 0 to 4.3 to investigate its effect on fabric development and creep rheology. Creep tests began at a shear stress of ~70% of τ_{res} and shear stress was increased in steps equal to 2%, 5%, or 7.5% of τ_{res} and held for 45 min (Table 1). For experiments that did not reach steady shear strength during γ_i, τ_{res} was estimated using an average value from other experiments [*Rathbun et al.*, 2008] and then checked after creep loading.

[18] We measured frictional rheology and layer thicknesses changes at each stress until tertiary creep occurred (Figure 3). For shear stresses <90% of τ_{res}, shear strain was negligible during creep step tests [*Rathbun et al.*, 2008]. However, tertiary creep produced measurable shear strain for stresses near τ_{res}, as shown for the final stress step in Figure 3; note that about 18 ks in Figure 3a corresponds to $\gamma \sim 1.2$ in Figure 3b. For the conditions of our study, tertiary creep began at 92–100% of τ_{res}, depending on γ_i [*Rathbun et al.*, 2008].

[19] After completion of the creep portion of the experiment, layers were again sheared at a constant displacement rate of 10 μm/s to investigate strain hardening and changes in friction (Figure 3a). The difference in frictional strength before and after creep was always <1.5%, and thus we assume that the strain accumulation during creep tests did not significantly affect fabric development.

[20] Details of the creep behavior during stress steps are given in Figure 4. The stress step risetime was 1–2 s, during which time shear strain rate increased rapidly. Layer dilation is clearly evident in the raw data dashed line (Figure 4), but to improve measurement precision, we removed the trend in layer thickness associated with geometric thinning [*Scott et al.*, 1994]. For a step increase in stress, strain rate first increased, consistent with primary creep, and then decayed steadily to a steady state value within 30–40 min (Figure 4, inset), which we associated with secondary creep. We did not attempt to verify the establishment of secondary creep in each case, because many previous works have shown that friction of geomaterials exhibits log-time creep relaxation for subcritical stresses [e.g., *Marone*, 1998; *Karner and Marone*, 2001; *Mitchell and Soga*, 2005; *Rathbun et al.*,

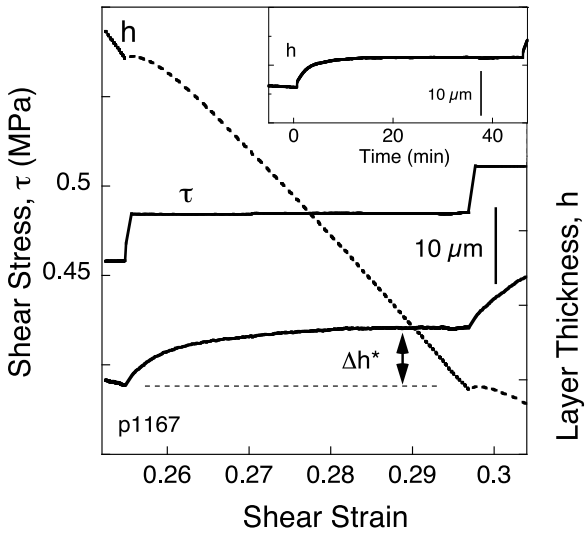

Figure 4. Layer thickness data for two representative shear stress steps during creep loading. Dashed line shows raw layer thickness. Lower line shows change in layer thickness, Δh^* corrected for geometric thinning. Note rapid dilation and steady state change in thickness caused by stress steps. Inset shows the temporal evolution of corrected layer thickness during one complete stress step.

2008]. However, for the resolution of our measurements (<0.1 μm), layer dilation was complete within 10–20 min after a stress step (Figure 4, inset). We define creep dilation Δh^* as the difference between layer thickness 40 min after the stress step and initial layer thickness before the step. Positive Δh^* represents dilation. The values of Δh^* do not vary systematically as a function of shear stress in a given experiment.

3.2. Dilation and the Onset of Localization

[21] We investigated the effect of shear localization on creep behavior by systematically varying preconditioning shear strain γ_i (Figure 3). Figure 5 shows data from 12 experiments in which we compare creep dilation as a function of stress step magnitude and shear strain. Our three stress step magnitudes range from 0.01 to 0.045 MPa (Figure 5). Layer dilation Δh^* increased strongly with stress change for layers with low initial strain ($\gamma_i < 0.2$), whereas for higher values of γ_i, dilation was nearly independent of stress step size (Figure 5).

[22] To further investigate shear localization and fabric development, we analyzed the effect of stress perturbations on layer thickness Δh^* (e.g., Figure 4) as a function of γ_i (Figure 6). The dilation parameter Δh^* is a proxy for fabric development if dilation occurs within only the fraction of the layer thickness where strain is localized. Figure 6 shows data for three layer thicknesses and two normal stresses. For our range of conditions, Δh^* did not vary systematically with normal stress (Table 1). Each point in Figure 6 represents the average of all shear stress steps in a given experiment plotted versus γ_i (e.g., Figure 3).

[23] The bulk of our experiments were conducted using 1 cm thick layers. In these experiments, creep dilation decreased systematically as a function of initial shear strain and reached stable values by $\gamma_i \sim 1.2$–2 (Figure 6). Layer dilation was about 6 μm for $\gamma_i = 0.1$ (the lowest values we could study) and decreased to 1 μm for $\gamma_i \geq 1.2$. These data are consistent with a logarithmic decrease in Δh^* as a function of γ_i, at least up to $\gamma_i = 1.2$. Beyond $\gamma_i = 1.2$, dilation remains constant with increasing shear strain (Figure 6, inset).

[24] A subset of experiments was conducted with 0.3 or 0.5 cm thick layers (Figure 6). For the thinner layers, layer dilation was about 3 μm for the lowest γ_i, values and decreased to 2 μm for $\gamma_i = 1$. These data are consistent with the idea that shear is distributed across the entire layer thickness at low strains and then becomes localized, to a thickness that is independent of h, for larger strains. Shear localization and fabric development also influence the rheology of sheared granular layers [*Rathbun et al.*, 2008]. In section 3.3, we extend the investigation of shear localization and consider results from tests conducted at constant macroscopic strain rate (e.g., Figure 3).

3.3. Slip Velocity Step Tests

[25] In addition to velocity step tests conducted after creep mode loading (e.g., Figure 3), we ran dedicated experiments at controlled shear velocity, which included stepwise increases and decreases in velocity between 10 and 30 μm/s (Figure 7). These experiments were done with 10 mm thick layers and were designed to assess variations in rate/state friction parameters as a function of strain. Such variations have been used as a proxy for fabric development in sheared layers [*Marone and Kilgore*, 1993; *Beeler et al.*, 1996]. The shear displacement at each velocity was 450 or 550 μm (Table 1). Velocity steps continued until a maximum displacement of ~35 mm corresponding to shear strains of 3.5–4. During the initial phase of shear stress increase, velocity steps were partially obscured by nonlinear strain hardening (Figure 7).

[26] After friction reached steady state, we imposed step changes in load point velocity, which caused variations in

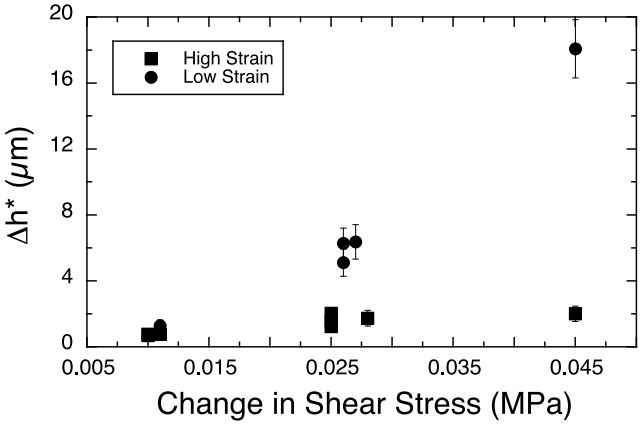

Figure 5. Scaling of dilation Δh^* with magnitude of shear stress change. Note that Δh^* increases with stress step size for low shear strain ($\gamma_i < 0.2$) but not for higher shear strain. High strain corresponds to $\gamma_i = 1$–1.2 for 0.01 and 0.025 MPa steps and $\gamma_i = 1.28$ for 0.045 MPa steps. Low strain corresponds to $\gamma_i < 0.02$ for 0.01 and 0.025 MPa steps and $\gamma_i = 0.026$ for 0.045 MPa steps.

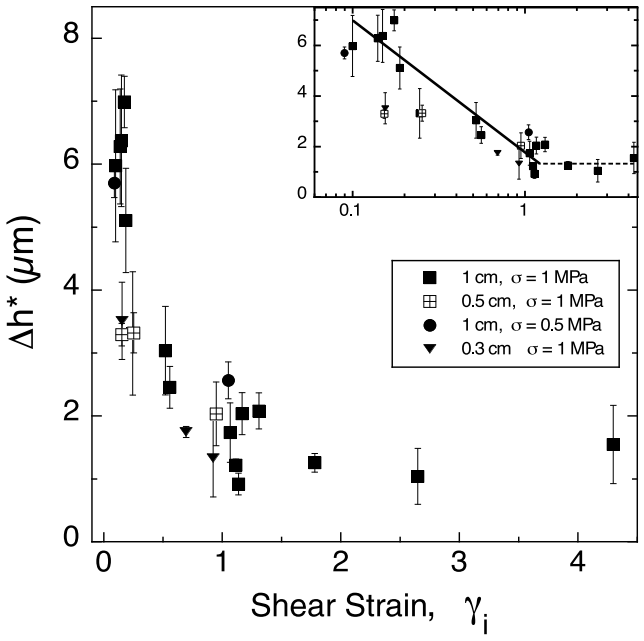

Figure 6. Layer dilation Δh^* induced by shear stress perturbations of magnitude 0.05 τ_{res} (e.g., Figure 4) plotted versus γ_i, the initial shear strain prior to creep tests (e.g., Figure 3). Inset shows data versus the log of γ_i. Dilation is largest at low γ_i, where shear is expected to be pervasive, and decreases systematically as a function of γ_i. The 0.5 cm thick layers show about half the dilation of 1 cm thick layers at low strain, about 3 and 6 μm, respectively, but the values are about the same for a shear strain of 1. Each data point represents several stress steps. Error bars show one standard deviation from the mean and data with error >30% of the mean are not plotted.

sliding friction (Figure 7, inset). Upon an increase (decrease) in loading velocity, friction increased (decreased) and then decayed to a new steady over a critical slip distance, D_c (Figure 7). The dependence of friction on slip rate and state (recent slip history) can be described by the rate and state friction relation

$$\mu \equiv \mu(V,\theta) = \mu_0 + a\ln\left(\frac{V}{V_0}\right) + b\ln\left(\frac{V_0\theta}{D_c}\right) \tag{2}$$

and one of two evolution laws for the friction state variable [*Dieterich*, 1979; *Ruina*, 1983]

$$\text{Dieterich law} \qquad \frac{d\theta}{dt} = 1 - \frac{V\theta}{D_c}, \tag{3a}$$

$$\text{Ruina law} \qquad \frac{d\theta}{dt} = -\frac{V\theta}{D_c}\ln\left(\frac{V\theta}{D_c}\right), \tag{3b}$$

where μ is the friction coefficient, μ_0 is friction at a reference velocity V_0, V is the sliding velocity, θ is a state variable, and a and b are dimensionless constants (Figure 7, inset). The friction parameters a, b, and D_c are obtained by solving the coupled equations (2) and (3a) or (3b) along with a description of elastic interaction with the testing machine

$$\frac{d\mu}{dt} = k(V_l - V), \tag{4}$$

where k is apparatus stiffness divided by normal stress and V_l is load point velocity [e.g., *Marone*, 1998].

[27] In our experiments, we observed that a step increase in loading velocity causes a rapid increase in shear stress. The rate of stress increase with load point displacement is equal to the system stiffness (Figure 7). At some point, the stress becomes sufficient to cause further slip within the layer and then frictional strength reaches a maximum, after which it decays to a new steady value (Figure 7, inset). The *e*-folding distance required to establish the new steady state sliding friction is the critical slip distance D_c. We observe that decreases in loading rate cause a sudden drop in frictional stress, followed by strengthening to a new steady state level. When the steady state change in friction has the same sign as the velocity change, such as shown in Figure 7, the material is said to exhibit velocity strengthening frictional behavior. Velocity weakening frictional behavior is defined by a lower steady state friction value at higher sliding velocity. Friction rate dependence is given by

$$a - b = \frac{\Delta\mu_{ss}}{\Delta\ln V}. \tag{5}$$

[28] Previous works on granular and clay fault gouge have shown that negative values of the friction rate parameter, $a - b$, are associated with localized shear [*Marone et al.*, 1990, 1992; *Beeler et al.*, 1996]. As fabric develops and shear becomes more localized, the critical slip distance decreases [*Marone and Kilgore*, 1993]. According to *Marone and Kilgore* [1993], the reduction in D_c occurs because a smaller fraction of the bulk layer and fewer particle-particle contacts are contributing to shear.

3.4. Evolution of the Critical Slip Distance

[29] We analyzed velocity step tests to assess evolution of constitutive parameters with strain and fabric development (Figure 7). A nonlinear, least squares inversion method was used to obtain parameters, following the procedures of *Blanpied et al.* [1998]. Each velocity step was modeled separately (Figure 8). In a few cases, the data exhibit a small overall trend of strain hardening (or weakening), which we accounted for by including a linear term in the model. The best fit model and a sensitivity analysis for the critical slip distance, D_c, are presented for two representative velocity steps in Figure 8 using both the Dieterich state evolution law (equation (3a)) and the Ruina evolution law (equation (3b)). For the velocity increase, the best fit parameters are: a = 0.0116, b = 0.0106, and D_c = 95 μm using the Dieterich law and a = 0.0121, b = 0.0102, and D_c = 115 μm using the Ruina law (Figure 8). For the velocity decrease, the best fit parameters are a = 0.0137, b = 0.0117, and D_c = 152 μm, and a = 0.0131, b = 0.0110, and D_c = 108 μm for the Dieterich and Ruina laws, respectively (Figure 8). For reference, we fix the values of a and b in each case and compute three forward models using different values of D_c. Changing the

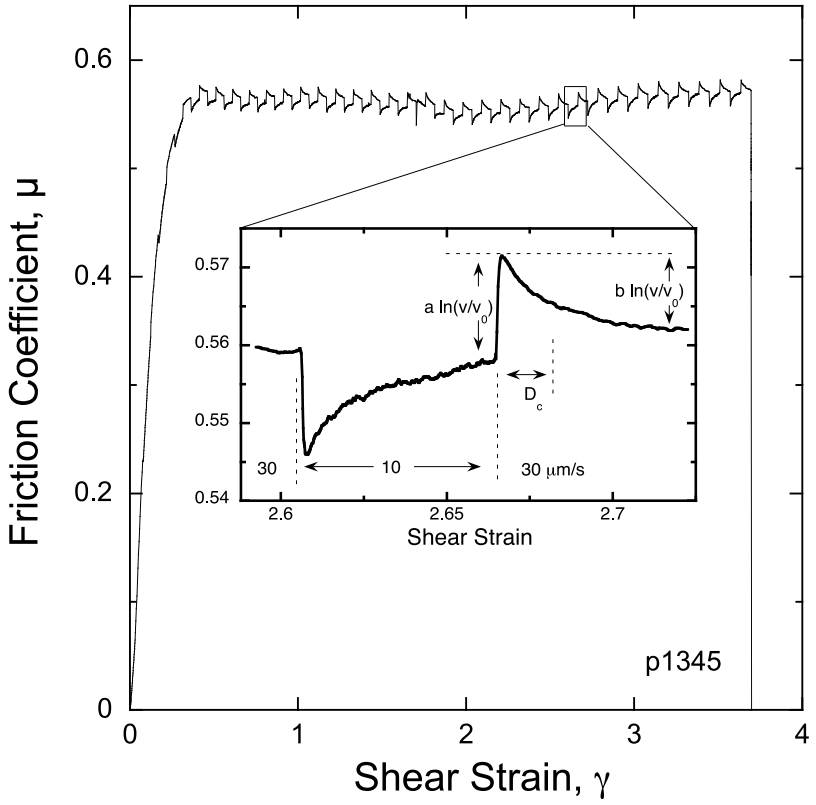

Figure 7. Controlled slip velocity experiment. Velocity is stepped between 10 and 30 μm/s and held for either 450 or 550 μm for the entire displacement range of the apparatus. Each velocity step causes a spike, then decay in friction. Inset shows frictional response to a step increase in velocity. When velocity is increased, frictional strength increases instantaneously and then decays over a characteristic slip distance (D_c). In this example, the instantaneous increase is larger than the subsequent decay, and therefore the steady state sliding friction exhibits positive $a - b$ and velocity-strengthening behavior.

value of D_c by as little as 25 μm results in a significant misfit (Figure 8).

[30] Comparison of forward models with similar values of D_c shows that the friction behavior is asymmetric for velocity increases and decreases when analyzing the steps with Dieterich evolution. The value of D_c is nearly a factor of 2 higher for velocity decreases compared to increases. Whereas the values of D_c are symmetric when the data are fit using the Ruina law. There is significant covariance between parameters [e.g., *Blanpied et al.*, 1998], but we focus here on D_c, for fixed values of a and b, to assess asymmetry and differences between velocity increases and decreases.

[31] Using the procedure shown in Figure 8, we assess evolution of constitutive behavior as a function of shear strain by fitting velocity steps for multiple experiments. Values of $a - b$ are similar for velocity increases and decreases, with both showing velocity strengthening and a slight reduction in magnitude for $\gamma < 2$ (Figure 9). The average value of $a - b$ for velocity increases is 0.0023 ± 0.0014 compared to 0.0028 ± 0.0019 for velocity decreases with the Dieterich law. Using the Ruina law, these values change slightly to 0.0022 ± 0.0014 and 0.0024 ± 0.0016 for increases and decreases, respectively. This consistency is expected because $a - b$ represents a steady state response, which is independent of the details of state evolution. Our measurements are consistent with previous results for this material [*Rathbun et al.*, 2008], which show velocity strengthening frictional behavior for normal stresses from 50 kPa to 5 MPa and slip velocities from 1 to 300 μm/s.

[32] Considering the range of our data, which start at a shear strain of about 1, the critical slip distance is independent of shear strain, within the scatter in the data. However, D_c is systematically different for velocity increases and decreases (Figures 9a and 9c) when using the Dieterich law. Mean values of D_c are 93.3 ± 20.2 μm and 182.9 ± 41.1 μm for velocity increases and decreases, respectively, in experiment p1572. These data and the sensitivity analysis of Figure 8 show a clear asymmetry in the critical slip distance for step increases and decreases in velocity. Friction approaches steady state within a shorter slip distance after velocity increases than velocity decreases.

[33] We modeled the same velocity steps with the Ruina state evolution law and find that the values of D_c are symmetric for velocity increases/decreases (Figure 9). In experiment p1572, the mean for D_c is 122 ± 53 μm and 140 ± 18 μm for velocity decreases and increases, respectively. In p1345, increases have a D_c of 139.1 ± 34.7 μm and decreases a D_c of 131 ± 19 μm when using the Ruina law. For experiment p1507, the mean for increases is 123 ± 29 μm and for decreases 121 ± 13. There is no clear asymmetry within the scatter in these data.

[34] In all cases, the Dieterich law produces significant asymmetry for velocity increases/decreases. This is consis-

tent with expectation, because the Dieterich law assumes that steady state is reached within a critical time; thus, the slip that accumulates during that time should be larger for velocity increases than for velocity decreases. This would predict larger values of D_c for velocity increases than decreases, which is opposite to what we observe (Figure 9). This issue is discussed in section 4.2.

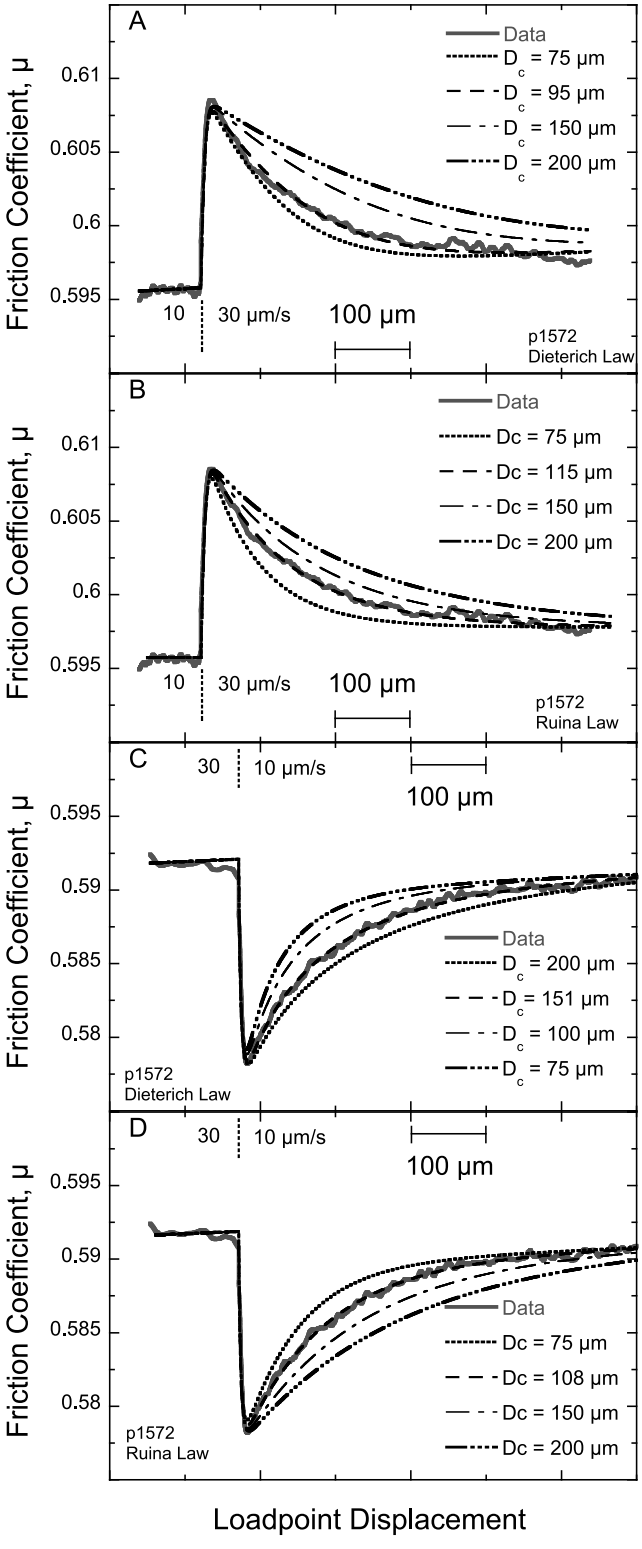

3.5. Strain Markers and Localized Deformation

[35] Thin zones of blue sand were added to select experiments (Table 1) to track the strain distribution within the layer. These layers were carefully recovered after shear, impregnated with a low-viscosity epoxy, and cut to expose a plane perpendicular to the layer and parallel to the shear direction (Figure 10). Photomicrographs in reflected light document offset of the markers and a combination of pervasive and localized strain (Figure 10). These images confirm that shear occurred within the sample and not at the interface with the rough forcing blocks. Strain markers are arcuate near the layer edges and curve into a boundary parallel (Y) orientation toward the center of the layer (Figure 10b). The thin zone of shear marker seen throughout the layer indicates that strain does not localize into a true Y shear, but into a narrow zone in the center of the sample. This implies that the boundary parallel "Y shears" in these experiments have finite width and that shear within them is not on an infinitesimally thin plane.

[36] Curvature of the markers along the layer boundaries indicates progressive localization with increased macroscopic strain (Figures 10b–10d). Three transects were taken across the sheared sample, one at each boundary and one in the center of the shear marker (Figure 10c). The angular shear strain

$$\gamma_a = \tan \psi, \tag{6}$$

where ψ is the angle between the initial position of the shear marker and current position, and was calculated in the curved portion of the marker using the method of *Ramsay and Graham* [1970]. The γ_a can be calculated between each point along the transect (Figure 10d). We may compare angular shear strain, γ_a, to bulk shear strain across the layer, γ (equation (1)). Bulk shear strain represents a macroscopic average whereas γ_a can be used to infer strain in a localized area of the sample and may have values much larger than γ. We only present calculations of γ_a along the curved portion of the strain marker, near the layer boundary (Figures 10c and 10d). In the central, high-strain portion of the layer, Riedel shears and indentations of large grains into our shear marker preclude calculations of γ_a.

Figure 8. Two velocity steps with velocity increased (Figures 8a and 8b) and decreased (Figures 8c and 8d) for experiment p1572. (a) Velocity is instantaneously increased from 10 to 30 μm/s. After the increase, friction increases and then decays to a new steady value over the critical slip distance (D_c). Inverse modeling using the Dieterich law (thick, gray line) produces values of 0.0116, 0.0106, and 94.7 μm for the parameters a, b, and D_c, respectively. Forward models with different values for the critical slip distance are shown for reference. (b) Analysis using the Ruina law. Inverse modeling produces values of 0.0121, 0.0102, and 114.7 μm for a, b, and D_c, respectively. (c) Velocity is decreased to 10 μm/s and modeled with the Dieterich law. Values are 0.0137, 0.0117, and 151.5 μm for a, b, and D_c, respectively. Reference forward models are shown for different critical slips. (d) Velocity decrease modeled with the Ruina law. Values are 0.0131, 0.0110, and 108.0 μm for a, b, and D_c, respectively.

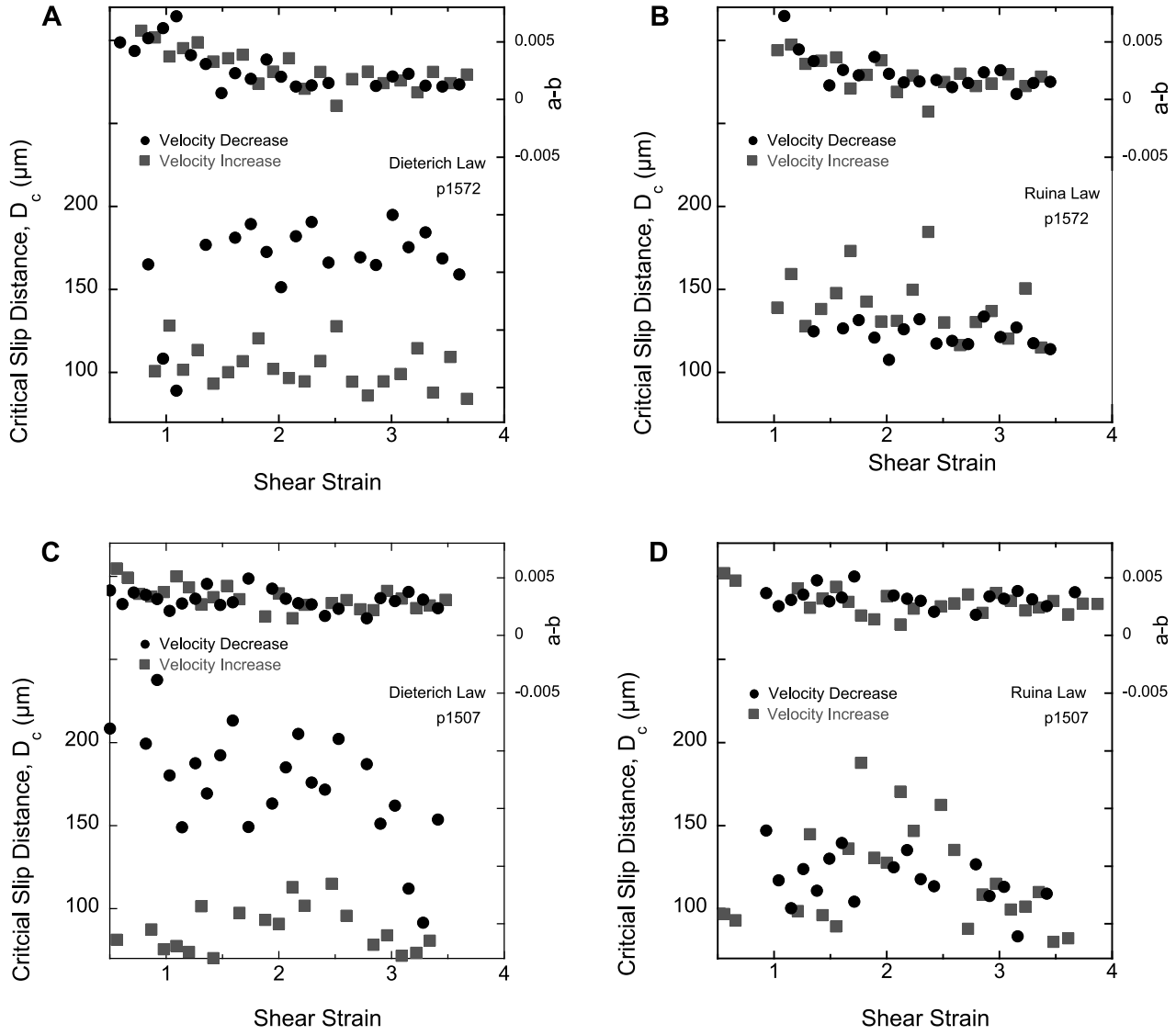

Figure 9. Friction constitutive parameters for two select experiments. Velocity decreases and increases are presented for the (a, c) Dieterich law and (b, d) Ruina law. The velocity dependence of friction ($a - b$) decreases with increased shear strain in all cases. Values for $a - b$ show no variation between velocity increases or decreases when using either law. Values of the critical slip distance are dependent on the sign of the velocity step when modeled with the Dieterich law (Figures 9a and 9c). Modeling the data with the Ruina law produces equivalent D_c for both velocity increases and decreases.

[37] Figure 10d presents γ_a as a function of position within the sample. Near the shear zone boundary, γ_a is near zero and increases toward the center of the layer. Strain is high in the central zone and local variations associated with large grains and slip surfaces make it difficult to resolve the peak strain value. Thus, equation (6) does not give an accurate assessment of strain in the central region. Nevertheless, the overall strain distribution can be approximated with a normal distribution and compared to measurement of macroscopic layer strain, γ, from the experiment. We integrate the normal distribution to derive a total shear displacement of 16.6 mm. The value can be compared to the measured shear displacement imposed at the layer boundaries, which was 30.4 mm, and the bulk shear strain, which was 3.9. We may assume that the slip derived from local angular shear strain, 16.6 mm, represents only that which occurred outside the central zone of high strain (Figure 10). This amount of slip corresponds to the outer, curved portion of the shear marker. In this case, the remaining γ of 1.9 would occur in the central, boundary parallel section, which is roughly 1.6 mm thick and in the center of the sample. The 1.6 mm thickness corresponds to a few grain diameters in thickness. To account for the remaining γ in the layer, a peak shear strain of 8.6 is required for the highly localized section near the center of the layer, which is reasonable.

[38] Shear markers and the spatial distribution of strain in the layer show that shear is initially pervasive and becomes localized (Figure 11). One possibility is that *Y* shear formation could simply cut the markers as shown in Figure 11c. However, the photomicrographs document significant cur-

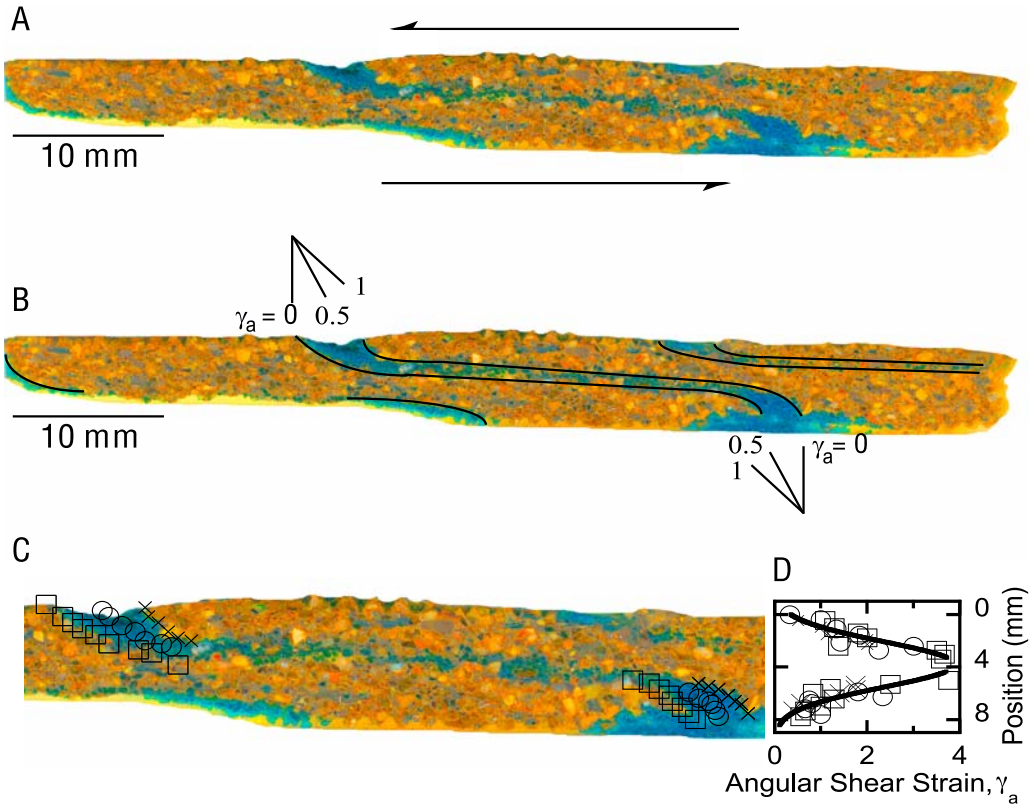

Figure 10. Photomicrograph showing shear strain within the layer. Total bulk shear strain in the experiment was 3.9. (a) The strain markers were initially vertical; arrows on the top and bottom indicate sense of shear. (b) The three sets of strain markers are outlined. Because of the large displacement in the sample, only the central marker is complete. During disassembly, the sample parted on the leftmost strain marker. The shear marker curves into a boundary parallel zone in the center of the sample. Fiducial lines represent the angular shear strain from the rotation of a vertical line. (c) Enlarged image of Figure 10a with three transects across the shear zone. The angular shear strain, γ_a, is calculated between each point and presented in Figure 10d. (d) Angular shear strain as a function of position across the sample. Data symbols and position correspond to Figure 10c and the thickness of the sample. The displacement from the overlaid normal distribution (solid black line) corresponds to bulk shear strain, $\gamma \sim 2$ leaving $\gamma \sim 1.9$ in the center 1.6 mm of the sample. Micrograph from experiment p1508; no vertical exaggeration.

vature of the markers as expected for spatially progressive localization (e.g., Figure 11d).

[39] We posit that boundary parallel shear localization begins on multiple surfaces and progresses to a certain point before one or more of the zones coalesce to form a master shear band. Our observations suggest that during the initial stages of localization; shear surfaces nearest the layer boundary arrest first, while those nearer to the center continue to shear. The low relative amounts of strain on the boundary, progressing to larger relative amounts of strain near the center of our sample, cause a curvature of the strain markers (Figure 10).

4. Discussion

[40] The results of this study document strain localization and systematic changes in frictional behavior as a function of accumulated shear strain. Creep mode tests and perturbations in shear stress level show consistent layer dilation for an increase in shear stress, and we use dilation as a proxy for shear localization within the layer. These results are consistent with previous works, but we add to those and extend the investigation to show how progressive fabric development affects frictional behavior. Our work on slip velocity perturbations compares velocity increases and decreases, and investigates symmetry in the frictional behavior.

4.1. Dilation as a Proxy for Shear Localization

[41] For granular materials, dilation occurs when shear-induced grain rearrangement causes a local increase in porosity [*Reynolds*, 1885; *Mead*, 1925]. Our measurements of macroscopic layer dilation form the basis for assessing shear localization and the relationship between fabric development and frictional behavior. We perform two tests of the hypothesis that layer dilation is a valid proxy for shear localization. These involve (1) experimentally varying initial layer thickness (Figure 6) and (2) using strain markers to document slip distribution within the layers (Figure 10). In addition, we can compare our dilation data to inferences about localization based on friction constitutive parameters (Figure 9).

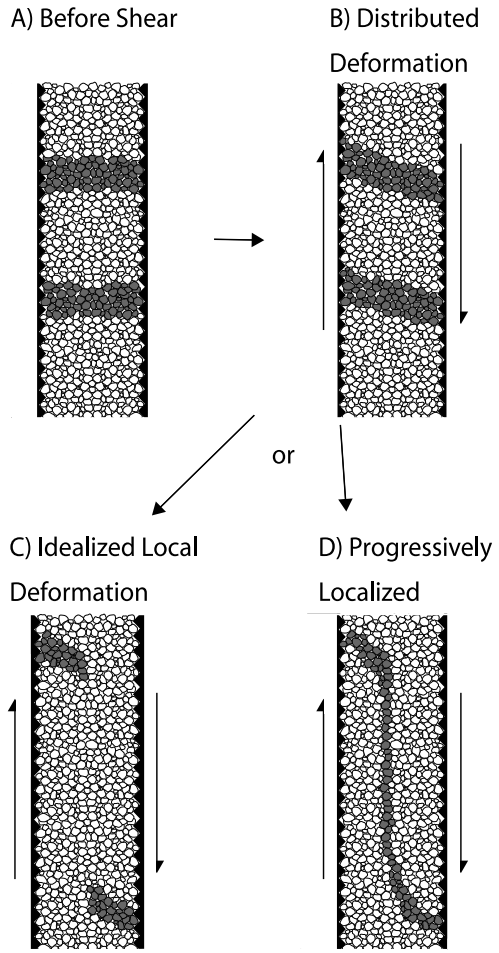

Figure 11. Idealized strain distribution for localized and distributed deformation. (a) Layer before shear with two theoretical strain markers. (b) During distributed deformation, passive strain markers are continuously offset in simple shear. (c) After initially distributed deformation, markers are offset by localized deformation in a thin zone or plane. (d) Distributed deformation transitioning into localized strain. Boundary zones stop contributing to layer deformation and neighboring grains continue to shear resulting in a slight offset of the marker. This process continues causing an apparent curvature of the strain marker until all shear occurs in the center of the sample.

[42] We varied initial layer thickness from 3 mm to 1 cm. Data for 1 cm thick layers show decreasing dilation with increasing shear strain (Figure 6). If this decrease is the result of shear localization, layer thickness will influence dilation at low strain, when deformation is pervasive, but at high strain, once deformation is localized, layer thickness will have no influence on dilation. Experiments on 0.3 and 0.5 cm layers produce half the dilation of 1 cm thick layers at $\gamma_i \sim 0.15$ (Figure 6), which is consistent with dilation throughout the layer (e.g., distributed shear). At $\gamma_i \sim 0.25$, our data are less convincing (Figure 6, inset). The 0.5 cm thick layers fall below the line defined by the 1 cm layers, but the data for 1 cm thick layers have large uncertainty (Figure 6, inset). At higher strains, when $\gamma_i = 1$, all layer thicknesses show equal dilation within experimental uncertainty and reproducibility. The large variability of dilation at γ_i suggests that localization may be complete at a slightly larger value than 1. These data are consistent with the hypothesis that deformation has localized into the same effective thickness for all macroscopic layer thicknesses. The micrographs and strain markers also support the conclusion that shear strain becomes localized within the layer for macroscopic shear strains in the range $\sim$1–2.

[43] Friction constitutive parameters have been used as a proxy for shear localization [e.g., *Marone and Kilgore*, 1993; *Beeler et al.*, 1996; *Scruggs and Tullis*, 1998; *Mair and Marone*, 1999; *Frye and Marone*, 2002; *Mitchell and Soga*, 2005]. *Marone and Kilgore* [1993] sheared layers of granular and powdered quartz and found that the critical slip distance D_c decreased until $\gamma \sim 6$. *Mair and Marone* [1999] investigated a range of normal stresses and slip rates and found that $a - b$ evolves until $\gamma \sim 4$. *Beeler et al.* [1996] conducted ring shear experiments on granular granite and found continued evolution of $a - b$ up to $\gamma > 50$.

[44] In our experiments, evolution of the friction constitutive parameters appears to be complete by $\gamma \leq 1$–2. The maximum γ we impose is $\sim$4, which is lower than other studies. Also, our material is a glacial till, with inherent heterogeneity of grains and a large-size distribution. We believe this is part of the cause of the scatter in D_c as well as Δh^* measurements. The values of $a - b$ display a clear evolution and decreasing trend until $\gamma \sim 2$ (Figure 9), consistent with localization assessed from the strain markers (Figure 10c). It is possible that continued strain would lead to further reduction of $a - b$. In the studies of *Marone and Kilgore* [1993], *Beeler et al.* [1996], and *Mair and Marone* [1999], most of the evolution of $a - b$ takes place at low strain, consistent with both our friction constitutive and creep dilation data.

[45] Laboratory studies of till localization using anisotropy of magnetic susceptibility (AMS) fabric indicate that localization evolves until γ on the order of 100 [*Larsen et al.*, 2006; *Thomason and Iverson*, 2006; *Iverson et al.*, 2008]. Unfortunately, these studies do not include data on the friction constitutive parameters for sheared till, and are all conducted in ring shear apparatuses. This configuration has a much lower stiffness than our apparatus and is typically used at lower normal stress. Thus, these tests require higher shear strain to reach steady state sliding friction, which makes direct comparison difficult. Past experiments on the tills used by *Thomason and Iverson* [2006] and *Iverson et al.* [2008] indicate velocity-weakening behavior, but without information on D_c or the evolution of friction constitutive parameters with strain [e.g., *Iverson et al.*, 1998]. In general, our results are consistent with these studies. We see that strain markers initially rotate in a manner consistent with distributed deformation and then record progressive localization in a narrow band of finite width, before slip localizes onto a surface that offsets the markers (Figure 10). The edges of the strain markers that were rotated during distributed deformation show both curvature and thinning toward the center of the shear zone, indicating that the transition to localized shear occurred progressively. It is possible that grains in our experiments continue to rotate and align into a higher-order preferred orientation than traditional shear fabrics. However, clast rotation and particle alignment are beyond the scope of this

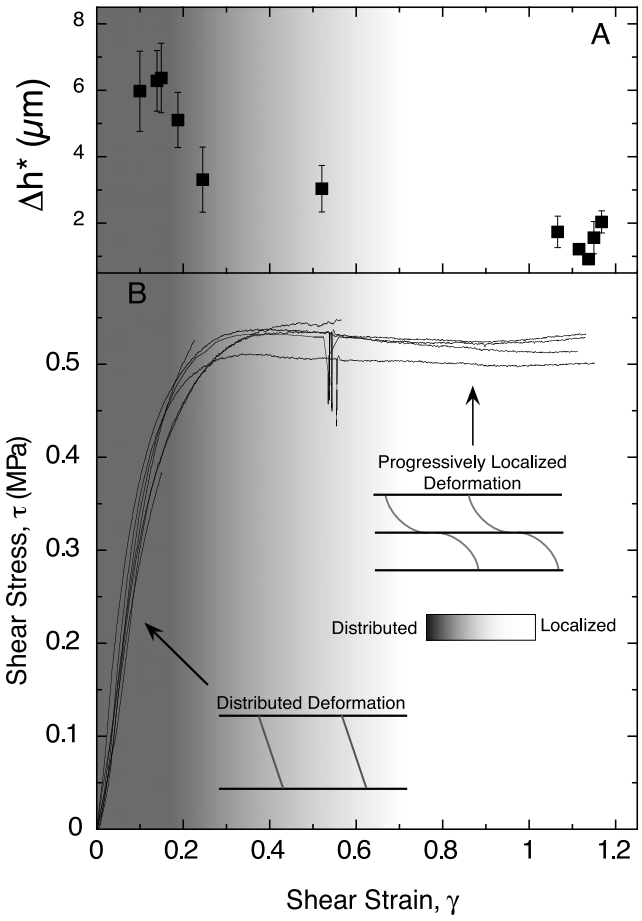

Figure 12. Layer dilation data with corresponding stress-strain curves for experiments at a normal stress of 1 MPa and initial layer thickness of 1 cm. (a) Dilation begins at $\gamma_i \sim 0.15$ and continues until $\gamma_i \sim 1$. During the low strain portion, distributed deformation is occurring throughout the layer. During the decrease in dilation, shear is progressing into the localized state. (b) This transition begins before the peak frictional strength and continues until after steady sliding friction has been achieved. Gray scale represents the progression from distributed shear (gray) to localized deformation (white).

study and we do not attempt to verify our results using preferred axis orientation.

[46] Our results are consistent with those of *Logan et al.* [1992], who sheared granular and clay-rich layers in the triaxial, sawcut configuration. They report pervasive deformation and the formation of oblique, Riedel shears during the initial, hardening portion of the stress-strain curve, followed by formation of boundary parallel *Y*-shears as frictional strength approaches steady state. *Scruggs and Tullis* [1998] also document localized shear in a boundary parallel zone within layers of mica and feldspar. They observe velocity-weakening frictional behavior and make a connection with shear localization and possible stick-slip instability.

[47] Strain markers in our experiments indicate that *Y*-shears have finite thickness and that they begin to form before the peak frictional strength (Figure 12). We find that dilation begins to decrease at $\gamma \sim 0.15$, which is before the peak shear strength (Figure 12). Dilation continues to decrease as the shear stress transitions to a steady sliding strength at $\gamma \sim 0.3$ in most experiments (Figure 12b). By $\gamma \sim 1.2$, the decrease in dilation is complete and sliding friction is steady. During the decrease in dilation, the mode of deformation changes from a distributed model to one in which most shear occurs in a boundary parallel zone in the center of the sample.

4.2. Symmetry of Frictional Behavior for Velocity Increases and Decreases

[48] In the context of rate and state friction, the two main state evolution laws (equations (3a) and (3b)) make different predictions regarding the symmetry of the response to velocity increases and decreases. The Ruina law predicts symmetric behavior while the Dieterich law predicts larger values of D_c for velocity increase than for velocity decrease. We model our results with both laws and find complex behavior. Our experiments show a clear asymmetry in the frictional response to velocity perturbations when data are fit using the Dieterich state evolution law. Moreover, the asymmetry is opposite to that predicted for the Dieterich law. The critical slip distance for velocity decreases are a factor of 2 larger than those for velocity increases (Figure 9), whereas they should be smaller, according to standard interpretation [e.g., *Marone*, 1998].

[49] Many previous studies of the evolution of rate/state friction with strain have focused on only velocity increases or decreases, without considering the question of symmetry. The experiments by *Marone and Kilgore* [1993] show decreasing D_c with increased shear strain in layers of granular quartz. They analyzed velocity decreases in detail and noted a similar trend for velocity increases; however, they did not compare velocity increases and decreases. The experiments of *Mair and Marone* [1999] find that D_c increases with velocity as predicted by the Dieterich law. *Marone and Cox* [1994] show that D_c increases with displacement for roughened gabbro blocks due to the production of a gouge zone. Within the reproducibility of their data, D_c is symmetric for velocity increases and decreases. Asymmetry of velocity increases and decreases has been observed in dilatancy produced by velocity steps [e.g., *Beeler et al.*, 1996; *Hong and Marone*, 2005].

[50] When data for velocity increases and decreases are compared directly, the frictional evolution we observe is indistinguishable for velocity increases and decreases (Figure 13a). This symmetry between the increase and decrease in velocity suggests that the Ruina law may be more appropriate for these data. This is in contrast to the work of *Beeler et al.* [1994] who performed experiments on granite and quartzite and showed that frictional state evolved primarily as a function of time, as predicted by the Dieterich state evolution law. For comparison, we present data from a second experiment showing asymmetry of the friction evolution (Figure 13b). For these data, pure quartz was sheared at a normal stress of 25 MPa. Velocity decreases appear to reach peak friction at smaller displacements than velocity increases, and friction evolves over a longer distance.

[51] Our data lend clear support for the Ruina law interpretation of frictional state evolution. However, an alternative hypothesis should be considered, given that we

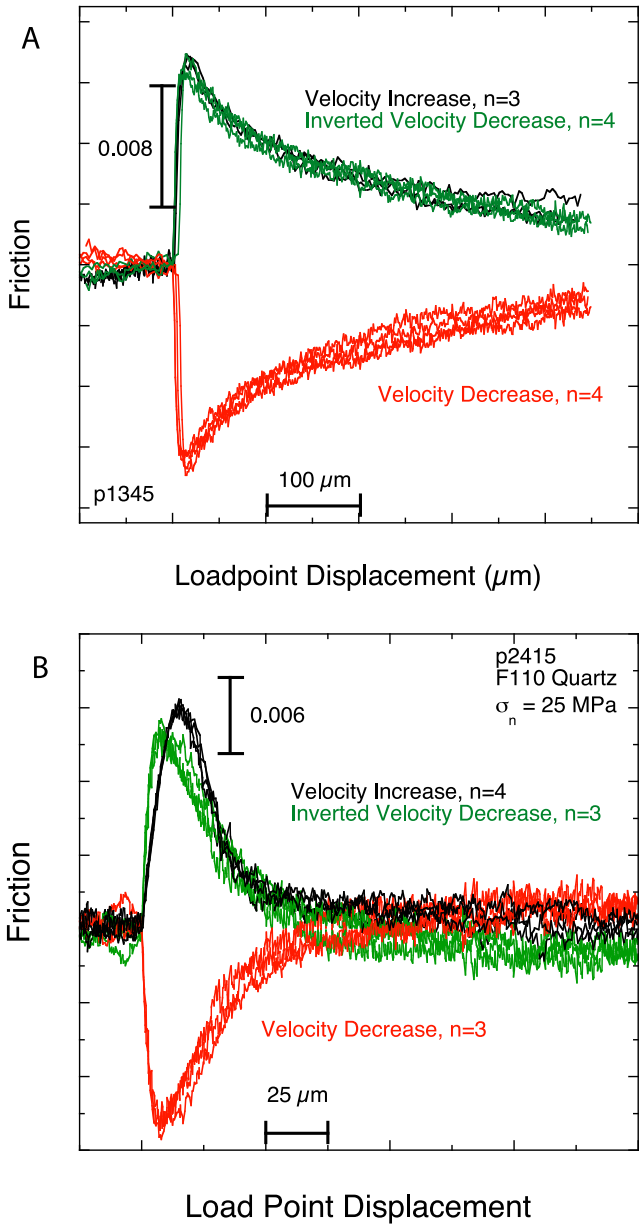

Figure 13. (a) Velocity increases and decreases for experiment p1345 on Caesar till at a normal stress of 1 MPa. Seven steps are shown: three velocity increases (black) and four decreases (red). Velocity decreases are inverted (green) for comparison. Peak friction and the evolution to steady state are indistinguishable for increases and inverted decreases. (b) Velocity increases and decreases for pure quartz sample shear at a normal stress of 25 MPa. Velocity increases and decreases exhibit differing behavior with the decreases reaching peak friction at smaller displacements and evolving to steady state and larger slip. Peak friction is slightly small for decreases than increases.

find evidence for shear localization in a gouge layer. One could argue that the Dieterich law is correct, and that changes in the degree of shear localization explain our data. Previous studies have established that the critical slip distance scales with particle size [e.g., *Dieterich*, 1981; *Marone and Kilgore*, 1993] in a manner consistent with *Rabinowicz*'s [1958] original interpretation of D_c in terms of the lifetime of adhesive contacts. *Marone and Kilgore* [1993] extended this idea and proposed that the critical slip distance for granular shear scales with the number of particles within a shear band (see also *Marone et al.*, 2009). That is, for a zone of thickness T, the effective critical slip distance D_{cb} is given by the sum of contributions from individual contacts within the zone

$$D_{cb} = nD_c\chi, \tag{7}$$

where χ is a geometric factor to account for contact orientation and n is the number of particle contacts in the shear band.

[52] For a fault zone of thickness T, the effective critical slip distance represents contributions from each contact within the zone. Particle diameter d can be related to D_c via contact properties as

$$D_c = d\,\zeta, \tag{8}$$

where ζ is a constant including elastic and geometric properties and the slip needed for fully developed sliding at the contact [*Boitnott et al.*, 1992]. Combining these relations and the constants yields a relation between D_{cb} and shear band thickness

$$D_{cb} = T\gamma_c, \tag{9}$$

where γ_c is the critical strain derived from slip increments on individual surfaces within the shear zone [*Marone and Kilgore*, 1993; *Marone et al.*, 2009].

[53] In the context of this model, asymmetry in frictional behavior for velocity increases versus decreases can be explained by dynamic variation in shear band thickness. Larger values of the effective critical slip distance imply that a larger number of contacts, and a thicker shear band, are actively slipping. Thus, we posit that a transient increase in the imposed shearing rate causes contacts to strengthen, via the friction direct effect, followed by weakening. This would cause a transient widening of the shear band, as interparticle slip is temporarily arrested and particles rotated, with attendant local dilation. With continued slip, and contact weakening via the friction evolution effect, the shear band would thin. We assume that interparticle contacts undergo velocity weakening, even where the macroscopic friction response is velocity strengthening [e.g., *Marone et al.*, 1990], and thus the shear band thins as slip is focused on weaker contacts. On the other hand, a transient decrease in the imposed shearing rate has the effect of, effectively, delocalizing shear by equalizing age (frictional state) of interparticle contacts within the active shearing zone relative to those outside the zone. This growth (thickening) of the actively shearing zone as it incorporated more material from "spectator" regions [e.g., *Mair et al.*, 2002; *Mair and Abe*, 2008] would produce larger D_{cb}.

4.3. Localization and Till Rheology

[54] The progressive localization that we observe is consistent with the changes in till rheology noted by *Rathbun et al.* [2008]. They observe a gradual change from

a pseudoviscous rheology with a stress exponent of order 1 at $\gamma \sim 0$, to values >30 as a function of accumulated shear strain. Our experiments were conducted using the same experimental configuration and on the same material as those of *Rathbun et al.* [2008]. The change in the stress exponent and the transition of the stress exponent occur over the same interval as our decrease in Δh^*. Our data support the idea that the rheology of till is a function of shear localization. These results suggest that as long as shear remains localized in till, a frictional (Coulomb-plastic) rheology is appropriate rather than a viscous rheology. In the case that pore pressure or some other feedback destroys localization, a viscous rheology could apply until shear strain accumulates.

5. Conclusions

[55] Laboratory experiments on a saturated, mixed grain size granular media show that shear begins to localize prior to the peak frictional strength. Dilation of the layer in creep experiments and the evolution of the friction constitutive parameters ($a - b$ and critical slip distance) all show a progressive transition from distributed shear to localized deformation. Passive strain markers in the layer confirm that distributed deformation occurs at the lowest shear strain, and then deformation occurs in a localized zone in the center of the sample. This localization occurs progressively starting at a strain of about 0.15 and continues after the peak strength until a shear strain of about 1–2. The localized zone is similar to boundary parallel *Y*-shears in the sample. Mapping shear strain across the deforming layer using embedded shear markers shows that the formation of the boundary parallel layer occurs at shear strain <1.9. These localization features occur despite the material showing velocity strengthening frictional behavior at all shear strains. Step increases and decreases in velocity indicate an asymmetry in some of the rate and state friction constitutive parameters. The asymmetry is observed in the critical slip distance, while the velocity dependence of friction remains constant for velocity increases and decreases when the data are modeled with the Dieterich law. If the data are modeled using the Ruina law, asymmetry is not observed or is obscured by scatter in the data owing to the heterogeneous nature of the material. Since the velocity dependence of friction remains constant for increases and decreases in velocity, asymmetry could be the result of changes in the degree of shear localization within the bulk layer. However, direct comparison of velocity increases and decreases shows nearly identical evolution of the critical slip distance, leading us to favor the Ruina law for friction state evolution.

[56] The results of this study imply that localization of strain can occur at low shear strains in preexisting faults and glacial deformation zones. The bulk rheology of subglacial till may be the result, and not the cause, of localization in the shearing till layer. Highly localized zones within fault gouge such as the principal slip surface may begin to form at low shear strain, regardless of velocity weakening or strengthening behavior.

[57] **Acknowledgments.** This work was funded by ANT-0538195. We thank Hitoshi Banno and Mike Underwood for providing XRD analysis. Particle size analysis was conducted at the Materials Research Institute, at Penn State. This manuscript was greatly improved by the comments of an anonymous reviewer, Chris Spiers and Associate Editor Dan Faulkner, comments on early versions by André Niemeijer and Sébastien Boutareaud and conversations on rate and state friction with Jon Samuelson.

References

Alley, R. B. (2000), Continuity comes first: Recent progress in understanding subglacial deformation, in *Deformation of Glacial Materials*, edited by A. J. Maltman, B. Hubbard, and M. J. Hambrey, *Geol. Soc. Spec. Publ.*, *176*, 171–179.

Anandakrishnan, S., and C. R. Bentley (1993), Micro-earthquakes beneath ice streams B and C, West Antarctica: Observations and implications, *J. Glaciol.*, *39*(133), 455–462.

Antonellini, M. A., and D. D. Pollard (1995), Distinct element modeling of deformation bands in sandstone, *J. Struct. Geol.*, *17*(8), 1165–1182, doi:10.1016/0191-8141(95)00001-T.

Arboleya, M. L., and T. Engelder (1995), Concentrated slip zones with subsidiary shears: Their development on three scales in the Cerro Brass fault zone, Appalachian valley and ridge, *J. Struct. Geol.*, *17*(4), 519–532, doi:10.1016/0191-8141(94)00079-F.

Beeler, N. M., T. E. Tullis, and J. D. Weeks (1994), The roles of time and displacement in the evolution effect in rock friction, *Geophys. Res. Lett.*, *21*(18), 1987–1990, doi:10.1029/94GL01599.

Beeler, N. M., T. E. Tullis, M. L. Blanpied, and J. D. Weeks (1996), Frictional behavior of large displacement experimental faults, *J. Geophys. Res.*, *101*(B4), 8697–8715, doi:10.1029/96JB00411.

Billi, A., and F. Storti (2004), Fractal distribution of particle size in carbonate cataclastic rocks from the core of a regional strike-slip fault zone, *Tectonophysics*, *384*, 115–128, doi:10.1016/j.tecto.2004.03.015.

Blanpied, M. L., C. Marone, D. A. Lockner, J. D. Byerlee, and D. P. King (1998), Quantitative measure of the variation in fault rheology due to fluid-rock interactions, *J. Geophys. Res.*, *103*(B5), 9691–9712, doi:10.1029/98JB00162.

Boitnott, G. N., R. L. Biegel, C. H. Scholz, N. Yosioka, and W. Wang (1992), Micromechanics of rock friction 2: Quantitative modeling of initial friction with contact theory, *J. Geophys. Res.*, *97*(B6), 8965–8978, doi:10.1029/92JB00019.

Boulton, G. S., and R. C. A. Hindmarsh (1987), Sediment deformation beneath glaciers: Rheology and geological consequences, *J. Geophys. Res.*, *92*(B9), 9059–9082, doi:10.1029/JB092iB09p09059.

Brace, W. F., and J. D. Byerlee (1966), Stick-slip as a mechanism for earthquakes, *Science*, *26*(153), 990–992, doi:10.1126/science.153.3739.990.

Carpenter, B. M. (2007), The transition from jamming to rolling in sheared granular media: The formation of force chains and effects of normal load and velocity, M.Sc. thesis, Dep. of Geosci., Pa. State Univ., University Park.

Cashman, S. M., and K. V. Cashman (2000), Cataclasis and deformation-band formation in unconsolidated marine terrace sand, Humboldt County, *Calif. Geol.*, *28*, 111–114.

Cashman, S. M., J. N. Baldwin, K. V. Casman, K. Swanson, and R. Crawford (2007), Microstructures developed by coseismic and aseismic faulting in near-surface sediments, San Andreas fault, *Calif. Geol.*, *35*, 611–614.

Chester, F. M., and J. S. Chester (1998), Ultracataclasite structure and friction processes of the Punchbowl fault, San Andreas system, California, *Tectonophysics*, *295*, 199–221, doi:10.1016/S0040-1951(98)00121-8.

Chester, F. M., J. S. Chester, D. L. Kirschner, S. E. Schulz, and J. P. Evans (2004), Structure of large-displacement, strike-slip fault zones in the brittle continental crust, in *Rheology and Deformation in the Lithosphere at Continental Margins*, edited by G. D. Karner et al., pp. 223–260, Columbia Univ. Press, New York.

Clarke, G. K. C. (2005), Subglacial processes, *Annu. Rev. Earth Planet. Sci.*, *33*, 247–276, doi:10.1146/annurev.earth.33.092203.122621.

Dieterich, J. H. (1979), Modeling of rock friction: 1. Experimental results and constitutive equations, *J. Geophys. Res.*, *84*(B5), 2161–2168, doi:10.1029/JB084iB05p02161.

Dieterich, J. H. (1981), Constitutive properties of faults with simulated gouge, in *Mechanical Behavior of Crustal Rocks*, *Geophys. Monogr. Ser.*, vol. 24, edited by N. L. Carter et al., pp. 103–120, AGU, Washington, D. C.

Di Toro, G., S. Nielsen, and G. Pennacchioni (2005), Earthquake rupture dynamics frozen in exhumed ancient faults, *Nature*, *436*, 1009–1012, doi:10.1038/nature03910.

Ekstrom, G., M. Nettles, and J. A. Abers (2003), Glacial earthquakes, *Science*, *302*(5645), 622–624, doi:10.1126/science.1088057.

Ekstrom, G. M., M. Nettles, and V. C. Tsai (2006), Seasonality and increasing frequency of Greenland glacial earthquakes, *Science*, *311*(5768), 1756–1758.

Engelder, J. T. (1974), Cataclasis and the generation of fault gouge, *Geol. Soc. Am. Bull.*, *85*, 1515–1522, doi:10.1130/0016-7606(1974)85<1515:CATGOF>2.0.CO;2.

Evans, D. J. A., E. R. Phillips, J. F. Hiemstra, and C. A. Auton (2006), Subglacial till: Formation, sedimentary characteristics and classification, *Earth Sci. Rev.*, *78*(1), 115–176, doi:10.1016/j.earscirev.2006.04.001.

Faulkner, D. R., A. C. Lewis, and E. H. Rutter (2003), On the internal structure and mechanics of large strike-slip fault zones: Field observations of the Carboneras fault in southeastern Spain, *Tectonophysics*, *367*, 235–251, doi:10.1016/S0040-1951(03)00134-3.

Fossen, H., R. A. Schultz, Z. K. Shipton, and K. Mair (2007), Deformation bands in sandstone: a review, *J. Geol. Soc.*, *164*(4), 755–769, doi:10.1144/0016-76492006-036.

Frank, F. C. (1965), On dilatancy in relation to seismic sources, *Rev. Geophys.*, *3*(4), 485–503, doi:10.1029/RG003i004p00485.

Frye, K. M., and C. Marone (2002), Effect of humidity on granular friction at room temperature, *J. Geophys. Res.*, *107*(B11), 2309, doi:10.1029/2001JB000654.

Gu, Y., and T.-F. Wong (1994), Development of shear localization in simulated quartz gouge: Effect of cumulative slip and gouge particle size, *Pure Appl. Geophys.*, *143*, 387–423, doi:10.1007/BF00874336.

Haefner, R. J. (1999), Field trip guide to selected fractured glacial till sites and soils in central Ohio, Conference on Fractured Glacial Tills, report, 27 pp., Water Manage. Assoc. of Ohio, Westerville.

Hayman, N. W., B. A. Housen, T. T. Cladouhos, and K. Livi (2004), Magnetic and clast fabrics as measurements of grain-scale processes within the Death Valley shallow crustal detachment faults, *J. Geophys. Res.*, *109*, B05409, doi:10.1029/2003JB002902.

Hong, T., and C. Marone (2005), Effects of normal stress perturbations on the frictional properties of simulated faults, *Geochem. Geophys. Geosyst.*, *6*, Q03012, doi:10.1029/2004GC000821.

Iverson, N. R., R. W. Baker, and T. S. Hooyer (1997), A ring-shear device for the study of till deformation: Tests on tills with contrasting clay contents, *Quat. Sci. Rev.*, *16*(9), 1057–1066, doi:10.1016/S0277-3791(97)00036-X.

Iverson, N. R., T. S. Hooyer, and R. W. Baker (1998), Ring-shear studies of till deformation: Coulomb-plastic behavior and distributed strain in glacier beds, *J. Glaciol.*, *44*(148), 634–642.

Iverson, N. R., T. S. Hooyer, J. F. Thomason, M. Graesch, and J. R. Shumway (2008), The experimental basis for interpreting particle and magnetic fabrics of sheared till, *Earth Surf. Processes Landforms*, *33*, 627–645, doi:10.1002/esp.1666.

Kamb, B. (1991), Rheological nonlinearity and flow instability in the deforming bed mechanism of ice stream motion, *J. Geophys. Res.*, *96*(B10), 16,585–16,595, doi:10.1029/91JB00946.

Kamb, B. (2001), Basal zone of the West Antarctic ice streams and its role in lubrication of their rapid motion, in *The West Antarctic Ice Sheet: Behavior and Environment*, *Antarct. Res. Ser.*, vol. 77 edited by R. B. Alley and R. A. Bindschadler, pp. 99–157, AGU, Washington, D. C.

Karner, S. L., and C. Marone (2001), Frictional restrengthening in simulated fault gouge: Effect of shear load perturbations, *J. Geophys. Res.*, *106*(B9), 19,319–19,337, doi:10.1029/2001JB000263.

Larsen, N. K., J. A. Piotrowski, and F. Christiansen (2006), Microstructures and microshears as a proxy for strain in subglacial diamicts: Implications for basal till formation, *Geology*, *34*(10), 889–902, doi:10.1130/G22629.1.

Logan, J. M., and K. A. Rauenzahn (1987), Frictional dependence of gouge mixtures of quartz and montmorillonite on velocity, composition, and fabric, *Tectonophysics*, *144*, 87–108, doi:10.1016/0040-1951(87)90010-2.

Logan, J. M., M. Friedman, N. Higgs, C. Dengo, and T. Shimamodo (1979), Experimental studies of simulated fault gouges and their application to studies of natural fault zones, in *Analysis of Actual Fault Zones in Bedrock*, edited by R. C. Speed and R. V. Sharp, *U.S. Geol. Surv. Open file Rep.*, *79-1239*, 305–343.

Logan, J. M., C. A. Dengo, N. G. Higgs, and Z. Z. Wang (1992), Fabrics of experimental fault zones: Their development and relationship to mechanical behavior, in *Fault Mechanics and Transport Properties of Rocks*, edited by B. Evans and T. Wong, pp. 33–68, Academic, London.

Mair, K., and S. Abe (2008), 3D numerical simulations of fault gouge evolution during shear: Grain size reduction and strain localization, *Earth Planet. Sci. Lett.*, *274*(1), 72–81, doi:10.1016/j.epsl.2008.07.010.

Mair, K., and C. Marone (1999), Friction of simulated fault gouge for a wide range of velocities and normal stress, *J. Geophys. Res.*, *104*(B12), 28,899–28,914, doi:10.1029/1999JB900279.

Mair, K., K. M. Frye, and C. Marone (2002), Influence of grain characteristics on the friction of granular shear zones, *J. Geophys. Res.*, *107*(B10), 2219, doi:10.1029/2001JB000516.

Mandl, G., L. N. J. de Jong, and A. Maltha (1977), Shear zones in granular material, an experimental study of their structure and mechanical genesis, *Rock Mech.*, *9*, 95–144, doi:10.1007/BF01237876.

Marone, C. (1998), Laboratory-derived friction constitutive laws and their application to seismic faulting, *Annu. Rev. Earth Planet. Sci.*, *26*, 643–696, doi:10.1146/annurev.earth.26.1.643.

Marone, C., and S. J. D. Cox (1994), Scaling of rock friction constitutive parameters: The effects of surface roughness and cumulative offset on friction of gabbro, *Pure Appl. Geophys.*, *143*, 359–385, doi:10.1007/BF00874335.

Marone, C., and B. Kilgore (1993), Scaling of the critical slip distance for seismic faulting with shear strain in fault zones, *Nature*, *362*, 618–621, doi:10.1038/362618a0.

Marone, C., C. B. Raleigh, and C. H. Scholz (1990), Frictional behavior and constitutive modeling of simulated fault gouge, *J. Geophys. Res.*, *95*(B5), 7007–7025, doi:10.1029/JB095iB05p07007.

Marone, C., B. E. Hobbs, and A. Ord (1992), Coulomb constitutive laws for friction: Contrasts in frictional behavior and localized shear, *Pure Appl. Geophys.*, *139*, 195–214, doi:10.1007/BF00876327.

Marone, C., M. Cocco, E. Richardson, and E. Tinti (2009), The critical slip distance for seismic and aseismic fault zones of finite width, in *Fault-Zone Properties and Earthquake Rupture Dynamics*, *Int. Geophys. Ser.*, vol. 94, edited by E. Fukuyama, pp. 135–162, Elsevier, New York.

Mead, W. J. (1925), The geologic role of dilatancy, *J. Geol.*, *33*, 685–698, doi:10.1086/623241.

Menzies, J., J. J. M. van der Meer, and J. Rose (2006), Till-as a glacial "tectomict," its internal architecture, and the development of a "typing" method for till differentiation, *Geomorphology*, *75*(2), 172–200, doi:10.1016/j.geomorph.2004.02.017.

Mitchell, J. K., and K. Soga (2005), *Fundamentals of Soil Behavior*, 3rd ed., John Wiley, Hoboken, N. J.

Montgomery, D. R., and D. L. Jones (1992), How wide is the Calaveras fault zone?: Evidence for distributed shear along a major fault in central California, *Geology*, *20*, 55–58, doi:10.1130/0091-7613(1992)020<0055:HWITCF>2.3.CO;2.

Mooney, W. D., and A. Ginzburg (1986), Seismic measurements of the internal properties of fault zones, *Pure Appl. Geophys.*, *124*, 141–157, doi:10.1007/BF00875723.

Morgan, J. K., and M. S. Boettcher (1999), Numerical simulations of granular shear zones using the distinct element method: 1. Shear zone kinematics and the micromechanics of localization, *J. Geophys. Res.*, *104*(B2), 2703–2719, doi:10.1029/1998JB900056.

Niemeijer, A. R., and C. J. Spiers (2005), Influence of phyllosilicates on fault strength in the brittle-ductile transition: Insights from rock analogue experiments, in *High-Strain Zones: Structure and Physical Properties*, edited by D. Bruhn and L. Burlini, *Geol. Soc. Spec. Publ.*, *245*, 303–327.

Rabinowicz, E. (1958), The intrinsic variables affecting the stick-slip process, *Proc. Phys. Soc. London*, *71*, 668–675, doi:10.1088/0370-1328/71/4/316.

Ramsay, J. G., and R. H. Graham (1970), Strain variation in shear belts, *Can. J. Earth Sci.*, *7*(3), 786–813.

Rathbun, A. P., C. Marone, R. B. Alley, and S. Anandakrishnan (2008), Laboratory study of the frictional rheology of sheared till, *J. Geophys. Res.*, *113*, F02020, doi:10.1029/2007JF000815.

Reynolds, O. (1885), On the dilatancy of media composed of rigid particles in contact, *Philos. Mag., Ser. 5*, *20*, 469–481.

Ruina, A. (1983), Slip instability and state variable friction laws, *J. Geophys. Res.*, *88*(B12), 10,359–10,370, doi:10.1029/JB088iB12p10359.

Schleicher, A. M., B. A. van der Pluijm, J. G. Solum, and L. N. Warr (2006), Origin and significance of clay-coated fractures in mudrock fragments of the SAFOD borehole (Parkfield, California), *Geophys. Res. Lett.*, *33*, L16313, doi:10.1029/2006GL026505.

Scholz, C. H. (1987), Wear and gouge formation in brittle faulting, *Geology*, *15*, 493–495, doi:10.1130/0091-7613(1987)15<493:WAGFIB>2.0.CO;2.

Scholz, C. H. (2002), *The Mechanics of Earthquakes and Faulting*, 2nd ed., Cambridge Univ. Press, Cambridge, U. K.

Scott, D., C. Marone, and C. Sammis (1994), The apparent friction of granular fault gouge in sheared layers, *J. Geophys. Res.*, *99*(B4), 7231–7246, doi:10.1029/93JB03361.

Scruggs, V. J., and T. E. Tullis (1998), Correlation between velocity dependence of friction and strain localization in large displacement experiments on feldspar, muscovite and biotite gouge, *Tectonophysics*, *295*, 15–40, doi:10.1016/S0040-1951(98)00113-9.

Sibson, R. H. (2003), Thickness of the seismic slip zone, *Bull. Seismol. Soc. Am.*, *93*(3), 1169–1178, doi:10.1785/0120020061.

Storti, F., A. Billi, and F. Salvini (2003), Particle size distributions in natural carbonate fault rocks: Insights for non-self-similar cataclasis, *Earth Planet. Sci. Lett.*, *206*, 173–186, doi:10.1016/S0012-821X(02)01077-4.

Thomason, J. F., and N. R. Iverson (2006), Microfabric and microshear evolution in deformed till, *Quat. Sci. Rev.*, *25*, 1027–1038, doi:10.1016/j.quascirev.2005.09.006.

Truffer, M., W. D. Harrison, and K. A. Echelmeyer (2000), Glacier motion dominated by processes deep in underlying till, *J. Glaciol.*, *46*(153), 213–221, doi:10.3189/172756500781832909.

Tsai, V. C., J. R. Rice, and M. Fahnestock (2008), Possible mechanisms for glacial earthquakes, *J. Geophys. Res.*, *113*, F03014, doi:10.1029/2007JF000944.

Underwood, M. B., N. Basu, J. Steurer, and S. Udas (2003), Data report: Normalization factors for semi-quantitative X-ray diffraction analysis, with application to DSDP Site 297, Shikoku Basin, *Proc. Ocean Drill. Program Sci. Results*, *190/196*, 1–26.

Wibberley, C. A. J., and T. Shimamoto (2003), Internal structure and permeability of major strike-slip fault zones: The Median Tectonic Line in Mie Prefecture, southwest Japan, *J. Struct. Geol.*, *25*, 59–78, doi:10.1016/S0191-8141(02)00014-7.

Winberry, J. P., S. Anandakrishnan, R. B. Alley, R. A. Bindschadler, and M. A. King (2009), Basal mechanics of ice streams: Insights from the stick-slip motion of Whillans ice stream, West Antarctica, *J. Geophys. Res.*, *114*, F01016, doi:10.1029/2008JF001035.

C. Marone and A. P. Rathbun, Rock and Sediment Mechanics Laboratory, Penn State Center for Ice and Climate, Pennsylvania State University, 513 Deike Bldg., University Park, PA 16802, USA. (arathbun@psu.edu; marone@psu.edu)